Subband electronic temperatures and electron-lattice energy relaxation in terahertz quantum cascade lasers with different conduction band offsets

Miriam S. Vitiello[a] and Gaetano Scamarcio
CNR-INFM Regional Laboratory LIT3, University of Bari, Via Amendola 173, 70126 Bari, Italy and Dipartimento Interateneo di Fisica "M. Merlin," Università degli Studi di Bari, Via Amendola 173, 70126 Bari, Italy

Vincenzo Spagnolo
CNR-INFM Regional Laboratory LIT3, University of Bari, Via Amendola 173, 70126 Bari, Italy and Dipartimento Interateneo di Fisica "M. Merlin," Politecnico di Bari, Via Amendola 173, 70126 Bari, Italy

Chris Worrall, Harvey E. Beere, and David A. Ritchie
Cavendish Laboratory, University of Cambridge, Madingley Road, Cambridge CB3 0HE, United Kingdom

Carlo Sirtori
Matériaux et Phénomènes Quantique Laboratory, Université Paris 7, 75251 Paris Cedex 05, France

Jesse Alton and Stefano Barbieri[b]
TeraView Limited, 302/304 Science Park, Cambridge CB4 OWG, United Kingdom and Cavendish Laboratory, University of Cambridge, Madingley Road, Cambridge CB3 0HE, United Kingdom

(Received 19 May 2006; accepted 8 August 2006; published online 28 September 2006)

The electronic temperatures of the conduction subbands, the local lattice temperature, and the electron-lattice energy relaxation times (τ_E) in bound-to-continuum $GaAs/Al_xGa_{1-x}As$ quantum cascade lasers, operating at 2.9 and 2 THz, are reported. This information has been gathered from the analysis of microprobe photoluminescence spectra collected during device continuous wave operation. We find that the electronic distributions in both the active region and the injector are thermalized and that all subbands share the same electronic temperature. The efficiency of electron cooling increases with the conduction band offset. © *2006 American Institute of Physics*.
[DOI: 10.1063/1.2357042]

Low frequency, compact and coherent terahertz sources are highly desirable for a wide range of applications, including imaging, sensing, and spectroscopy. THz quantum cascade lasers (QCLs) have shown considerable performance improvement since their demonstration[1] and operation at 2 or 1.9 THz (Refs. 2 and 3) has been recently achieved. How far the operating frequency can be further reduced still remains an open issue. One of the major obstacles is the fact that the transition energy becomes comparable to the subband broadening, hindering the selective injection, and extraction of carriers into the upper state and from the lower state of the laser transition, respectively.

In previous works, we have demonstrated how in bound-to-continuum (BTC) terahertz QCLs the inefficient electronic cooling, is an important cause of the performance degradation with temperature.[4] The energy relaxation is by far more efficient in resonant-phonon (RP) terahertz QCLs, thanks to the availability of electron-phonon scattering channels. However, in this class of devices the formation of a hot electron distribution in the upper radiative state is a key limiting factor for high temperature operation.[5] No experimental or theoretical study on the electronic temperature of the upper laser level in BTC terahertz QCLs has been reported so far.

In this letter we report on the subbands electronic (T_e^j) and local lattice (T_L) temperatures of far-infrared $GaAs/Al_xGa_{1-x}As$ BTC QCLs operating at 2.9 THz (sample A)[6] and 2 THz (sample B)[2] grown by molecular beam epitaxy with different Al mole fractions. We compare the electron-lattice energy relaxation rates and investigate the role of the conduction band offset on the electronic and thermal properties of terahertz QCLs.

The conduction and valence band structure of a single period of the investigated devices calculated at threshold for lasing are shown in Figs. 1(a)–1(d) for samples A and B. In both cases, the upper laser level consists of a single isolated subband, while the bottom state lies at the top of a group of closely spaced subbands. This scheme ensures the efficient electronic injection into the upper state via resonant tunneling and the fast depopulation of the lower state via elastic scattering. The active region of samples A (B) is 11.57 (14.02) μm thick and consists of 90 (110) periods of a $GaAs/Al_xGa_{1-x}As$ heterostructure.[2,6] In sample A (B) the Al mole fraction in the barriers is 15% (10%). In both cases, the optical waveguide relies on surface-plasmon modes formed at the interface between the top contact metallization and the semiconductor.[7] Identical mounting configurations have been used for both devices.

Our experimental method is based on microprobe band-to-band photoluminescence (PL) experiments carried out on devices operating in continuous waves both below and well above the laser threshold. We kept the laser induced electron heating below ~5 K by using an incident optical power density of ~6 kW/cm^2, thus maintaining the electronic distribution practically unperturbed.[8]

[a]Electonic mail: vitiello@fisica.uniba.it
[b]Present address: Matériaux et Phénomènes Quantique Laboratory, Université Paris 7, 75251 Paris Cedex 05, France.

 © 2006 American Institute of Physics
Downloaded 02 Oct 2006 to 193.204.188.4. Redistribution subject to AIP license or copyright, see http://apl.aip.org/apl/copyright.jsp

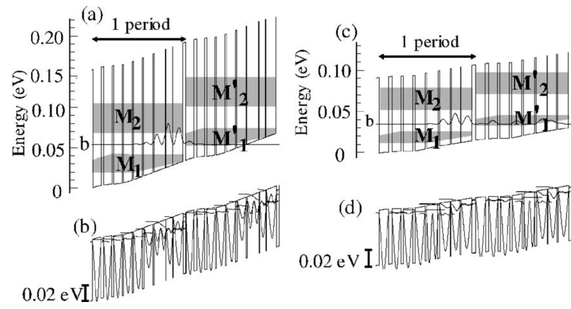

FIG. 1. Conduction (a-c) and valence (b-d) band structures of 2 periods of samples A (a)–(b) and B (c)–(d) calculated with a voltage drop of 27 mV (sample A) and 16 mV (sample B) per stage at the threshold for alignment. Starting from the injection barrier, the layer sequence for sample A in nanometers is (from right to left) **3.8**/14.0/**0.6**/9.0/**0.6**/15.8/**1.5**/12.8/**1.8**/12.2/**2.0**/12.0/**2.0**/11.4/**2.7**/11.3/**3.5**/11.6. For sample B, starting from the injection barrier, the layer sequence in nanometers is (from right to left) **5**/14.4/**1.0**/11.8/**1.0**/14.4/**2.4**/14.4/**2.4**/13.2/**3.0**/12.4/**3.2**/12.0/**4.4**/12.6. AlGaAs layers are shown in bold and the underlined GaAs wells are n doped at 1.6×10^{16} cm^{-3} (sample A) and 1.3×10^{16} cm^{-3} (sample B). The shaded area M_1 (M_1') represents the lowest energy miniband. M_2 (M_2') marks a higher energy miniband. The wave function square modulus of the excited laser state (bound level) is labeled b.

Figures 2(a) and 2(b) show a set of representative PL spectra measured in samples A and B for different values of the electrical power (P). In both cases, at zero bias, a single band associated with radiative transitions involving the injector miniband M_1 is present. Under bias, while electrons are tunnel injected into the upper laser level, additional features appear on the high energy tail of the PL band M_1. Furthermore, as a result of the combined effect of Joule heating and Stark shift induced by the applied electric field, M_1 shifts with P, as shown in the insets of Figs. 2(a) and 2(b) for samples A and B, respectively. The estimated electric field effect is a factor 1.4 times larger in sample A with respect to sample B, as expected considering the different designed biases.

The PL peaks labeled with b_{HH} in Fig. 2 correspond to heavy-hole (HH) excitonic transitions associated with level b.[4] A comparison between the PL spectra collected for samples A and B shows that, in the latter case, the intensity of the band b_{HH} is a factor of 3 lower. This can be explained by comparing the Debye screening length (λ_D) with the spatial extension of the wave function (l_b) associated with level b; while for sample A λ_D is in the range of 18–23 nm and $l_b\sim59$ nm, in the case of sample B, $15<\lambda_D<20$ nm and $l_b\sim42$ nm. Therefore, the screening effect is stronger in the latter case, thus reducing the intensity of excitonlike transitions. The PL bands labeled b are ascribed to band-to-band radiative transitions involving the upper laser level b. In Figs. 2(a) and 2(b) we also report the calculated energy position of the corresponding light-hole (LH) excitonic transition b_{LH}. The intensity ratio between LH and HH excitons is known to be strongly temperature dependent and can be as low as 10^{-2}–10^{-1} in the range 40–100 K.[9] Hence, the observation of LH excitons is hindered in our spectra. Finally, the high energy PL band in Fig. 2(a) is due to transitions involving the active region upper miniband M_2. Its presence can be explained in terms of thermally activated electron leakage from the top of the injector miniband M_1' nearly resonant with the bottom of M_2. This feature is absent in the spectra of sample B [Fig. 2(b)], since the lower operating bias ensures that the top of miniband M_1' is separated from the bottom of miniband M_2 by an energy greater than $k_BT_e^j$, where k_B is the Boltzmann constant. Also, the expected reduction of interface roughness scattering in sample B,[10] resulting from the use of a smaller Al mole fraction in the barriers, helps to reduce electron leakage.

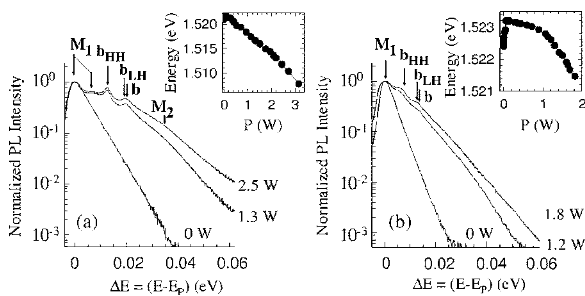

FIG. 2. Representative photoluminescence spectra of samples A (a) and B (b) measured at different P values, each plotted as a function of the energy difference ΔE with respect to the corresponding peak energy E_P of the low energy PL band M_1. The heat sink temperature is 45 K for sample A and 25 K for sample B. The arrows labeled M_j mark the energies of the transitions between levels in the conduction minibands (M_j) and valence subbands. The arrows marked with b_{HH} (b_{LH}) indicate the heavy-hole (light-hole) exciton peaks. The arrows indicated with b mark the energy of the transition between level b and a valence subband. Inset: Peak energy E_P of the PL band M_1 plotted as a function P. The lines are a guide for the eyes.

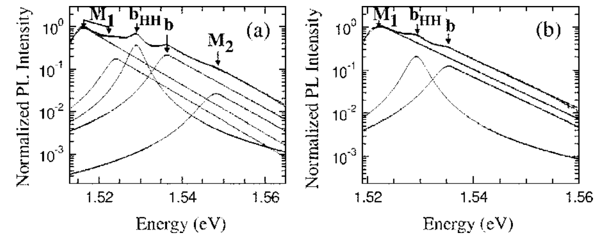

FIG. 3. Dashed line: photoluminescence spectrum at $P=1.5$ W (a) and at $P=1.6$ W (b) measured, respectively, for samples A and B. Solid line: calculated PL components peaked at the theoretical energies of relevant band-to-band transitions. The low-energy side of the curves labeled M_1, M_2, and b is a Lorentzian. The high-energy side is an exponential decay function $\propto\exp[E/k_BT_e^j]$. Curves relative to the b_{HH} transition are Lorentzians with a phenomenological broadening $\Gamma/2$. The experimental data have been fitted leaving $T_e^{M_1}$, $T_e^{M_2}$, T_e^b the band intensities and $\Gamma/2$ as fitting parameters.

In order to extract T_L, we have compared the redshift of the main PL peak as a function of P with that obtained by varying the heat sink temperature with the device at zero bias. The electronic temperatures T_e^j were extracted from the line shape analysis of each PL spectrum. For $P\geqslant1.15$ W, close to the threshold for lasing, an excellent reproduction of the PL is obtained by considering band-to-band transitions with an overlap integral of the envelope functions >0.25 and by leaving T_e^j, and the band intensities as fitting parameters. Figures 3(a) and 3(b) illustrate the application of this method to PL spectra collected at $P=1.5$ W (A) and $P=1.6$ W (B). The fitting procedure gives an upper value for the intensity ratio between LH and HH excitons of $\sim10^{-1}$ and $\sim10^{-3}$ for samples A and B, respectively. Accordingly, LH excitons have been disregarded.

The measured T_e^j and T_L values are plotted as a function of P in Figs. 4(a) and 4(b) for samples A and B, respectively. In case of sample B, we have restricted our analysis to $T_L>35$ K, where the variation of the energy gap with temperature ($dE_p/dT>0.3$ meV/K) leads to unambiguous evaluations. The electronic temperatures of the active region lower

Downloaded 02 Oct 2006 to 193.204.188.4. Redistribution subject to AIP license or copyright, see http://apl.aip.org/apl/copyright.jsp

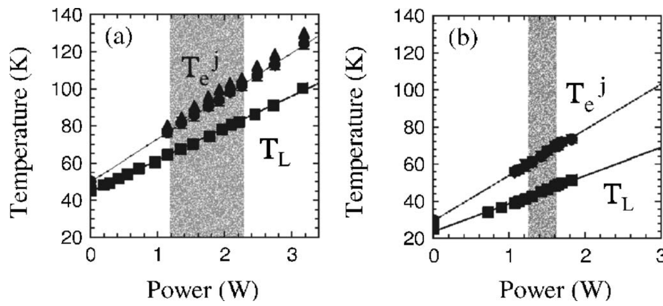

FIG. 4. Mean lattice temperature T_L (■) and subband electronic temperatures $T_e^{M_1}$ (●), T_e^b (▼) in the active region of samples A (a) and B (b) measured as a function of P with heat sink temperatures of 45 K and 25 K, respectively, for samples A and B. The lines are linear fits to the data. The shaded areas mark the lasing region.

energy levels increase linearly with P with the slopes $R_e^{(A)}=23.2$ K/W and $R_e^{(B)}=24.5$ K/W that are significantly larger than the corresponding thermal resistance values $R_L^{(A)}=17.3$ K/W and $R_L^{(B)}=15.6$ K/W. It is worth noting that the electronic temperatures of the upper laser level T_e^b and of the lower miniband M_1 are equal within $\sim$6 K (sample A) or $\sim$2 K (sample B). Moreover in sample A, the electronic temperature of the second miniband M_2 is nearly equal to that of M_1. This result demonstrates that, in BTC QCLs all the subbands share the same electronic temperature. This condition is potentially beneficial to obtain better device performance at high temperatures by reducing the increase with temperature of the nonradiative scattering rate from the upper laser level compared to the bottom level.

To compare the thermal properties of the investigated devices we have extracted the normalized thermal resistance $R_L^*=R_L\times S/d$, where S and d are the device area and the active region thickness, respectively.[7] We obtained $R_L^*(\mathrm{A})=37.4$ K cm/W and $R_L^*(\mathrm{B})=27.8$ K cm/W. We ascribe the lower value measured for sample B to (i) the lower Al concentration and (ii) the larger barrier and well thicknesses. Both these effects lead to the reduction of interface roughness scattering[11] thus increasing the thermal conductivity.[12]

From the measured R_e and R_L values we have extracted the electron-lattice energy relaxation time $\tau_E=[N_eNk_B(R_e-R_L)]$. In terahertz QCLs, the energy exchange rates between electrons and both optical and acoustic phonon subsystems contribute to τ_E. The results are reported in Table I, where we have included the values of τ_E measured in devices based on the same active region of sample A, but processed with metal-metal Au/Au (sample C) and In/Au (sample D) waveguide configurations.[13] The results for samples A, C, and D are practically coincident, demonstrating that the electron-lattice coupling is mostly determined by the quantum design of the gain medium. The τ_E value of sample B is larger by a factor of $\sim$1.6. This is mainly due to the reduced band-offset and to the reduced energy separation between the ground state level of the miniband M_1' and the top of the tunnel-injection barrier, $\sim$2 times lower in sample B with respect to sample A. Both these effects increase the number of thermally activated electrons leaking in the continuum, thus leading to an additional increase of the electronic temperature.[14] Although electron-electron interaction ensures the establishment of a thermalized hot electron energy distribution in each subband, the measured large τ_E values, are due to the lack of efficient electron-optical phonon relaxation channels.

TABLE I. Comparison between the electron-lattice energy relaxation times τ_E of a set of investigated terahertz QCLs, classified following their emission frequency (υ) and type of waveguide (Ref. 13) (*sp* and *m-m* represent a surface-plasmon and a double-metallic waveguide, respectively).

Sample	υ (THz)	Waveguide	τ_E (ps)
A	2.9	*sp*	3.7
B	2	*sp*	5.8
C[a]	2.9	*m-m* Au/Au	3.3
D[a]	2.9	*m-m* In/Au	3.6

[a]See Ref. 13.

In summary, in this letter we have shown that the use of a lower Al mole fraction and the related possibility to employ thicker barriers produce the reduction of interface roughness scattering, which leads to the enhancement of the active region thermal conductivity and thus improves the device thermal management. However, the use of a lower conduction band offset is disadvantageous for the electronic cooling. Our results demonstrate that the electron-lattice energy loss rate is not affected by the choice of the fabrication technology. Also, we observe that in BTC terahertz QCLs the electronic temperature of the upper radiative state is considerably reduced with respect to RP devices.[5] At the same time BTC terahertz QCLs show longer τ_E values. Therefore, a BTC active region scheme, modified by adding a phonon-depletion stage, is a potential solution to extend terahertz QCL operation at higher temperatures.

CNR-INFM acknowledges financial support from MIUR (DD 1105/2002). The University of Cambridge and Teraview Ltd. acknowledge financial support from the E.C. through the IST project Teranova and the PASR 2004 project Terasec. S.B. acknowledges support from the Royal Society.

[1]R. Köhler, A. Tredicucci, F. Beltram, H. E. Beere, E. H. Linfield, A. G. Davies, D. A. Ritche, R. C. Iotti, and F. Rossi, Nature (London) **417**, 156 (2002).
[2]C. Worrall, J. Alton, M. Houghton, S. Barbieri, H. E. Beere, D. A. Ritchie, and C. Sirtori, Opt. Express **14**, 171 (2006).
[3]S. Kumar, B. S. Williams, Q. Hu, and J. Reno, Appl. Phys. Lett. **88**, 121123 (2006).
[4]M. S. Vitiello, G. Scamarcio, V. Spagnolo, T. Losco, R. P. Green, A. Tredicucci, H. E. Beere, and D. A. Ritchie, Appl. Phys. Lett. **88**, 241109 (2006).
[5]M. S. Vitiello, G. Scamarcio, V. Spagnolo, B. S. Williams, S. Kumar, Q. Hu, and J. L. Reno, Appl. Phys. Lett. **86**, 11115 (2005).
[6]S. Barbieri, J. Alton, H. E. Beere, J. Fowler, E. H. Linfield, and D. A. Ritchie, Appl. Phys. Lett. **85**, 1674 (2004).
[7]Samples were processed into 250 μm wide ridge cavities by wet chemical etching the active region down to the top of the lower n^+ contact layer. Laser ridges of 1 mm long were defined by cleaving.
[8]M. S. Vitiello, G. Scamarcio, and V. Spagnolo, Proc. SPIE **6133**, 61330K (2006).
[9]R. Kumar, S. S. Prabhu, and A. S. Vengurlekar, Phys. Scr. **56**, 308 (1997).
[10]G. Scalari, S. Blaser, J. Faist, H. Beere, E. Linfield, D. Ritchie, and G. Davies, Phys. Rev. Lett. **93**, 237403 (2004).
[11]T. Unuma, M. Yoshita, T. Noda, H. Sakaki, and H. Akiyama, J. Appl. Phys. **93**, 1586 (2003).
[12]W. S. Capinski, H. J. Maris, T. Ruf, M. Cardona, K. Ploog, and D. S. Katzer, Phys. Rev. B **59**, 8105 (1999).
[13]M. S. Vitiello, G. Scamarcio, V. Spagnolo, J. Alton, S. Barbieri, C. Worral, H. E. Beere, D. A. Ritchie, and C. Sirtori Appl. Phys. Lett. **89**, 021111 (2006).
[14]V. Spagnolo, G. Scamarcio, W. Schrenk, and G. Strasser, Semicond. Sci. Technol. **19**, 1 (2004).

Downloaded 02 Oct 2006 to 193.204.188.4. Redistribution subject to AIP license or copyright, see http://apl.aip.org/apl/copyright.jsp